PREPRINT: P. Moonen, B. Blocken and J. Carmeliet, Indicators for the evaluation of wind tunnel test section flow quality and application to a numerical closed-circuit wind tunnel, International Journal of Wind Engineering and Industrial Aerodynamics, Vol. 95, pp. 1289-1314, 2007. (doi:10.1016/j.jweia.2007.02.027).

Indicators for the evaluation of wind tunnel test section flow quality and application to a numerical closed-circuit wind tunnel

Peter Moonen * [(a)], Bert Blocken [(a,b)], Jan Carmeliet [(a,b)]

(a) Laboratory of Building Physics, Department of Civil Engineering, Katholieke Universiteit Leuven, Kasteelpark Arenberg 40, 3001 Leuven, Belgium.
(b) Building Physics and Systems, Faculty of Building and Architecture, Technical University Eindhoven, P.O. box 513, 5600 MB Eindhoven, The Netherlands.

Abstract

The flow in a wind tunnel test section must meet high standards to obtain accurate and reliable measurement data. Good flow quality demands a certain degree of spatial uniformity and temporal steadiness of velocity and pressure. In this paper, a set of six new indices is developed and presented that relate spatial aspects of the mean velocity field to flow quality. One index quantifies the degree of uniformity of the velocity field and can be used directly as a flow quality indicator. The five other indices are related to different types of deviations from spatially uniform flow; skewed flow and angularity (up-flow and down-flow, swirl, cross-flow, diverging and converging flow). The indices can be used to evaluate the flow quality in existing tunnels, to assess the impact of design modifications, as well as to carry out CFD-based design of new wind tunnels. As an example, the indices are applied to assess the impact of guide vanes and screens on the test section flow quality in a numerical closed-circuit wind tunnel.

Keywords: Wind tunnel testing; Computational Fluid Dynamics; CFD; Numerical simulation; Wind flow; Air flow; Flow quality; Skewness; Up-flow; Down-flow; Cross-flow; Angularity; Uniformity.

1. Introduction

The vast amount of studies undertaken in wind tunnels and their importance for human life motivate the high demands that are posed on test section flow quality. Examples of wind tunnel studies in Wind Engineering are pedestrian wind comfort (Wu and Stathopoulos 1993; Richards et al. 2002), pollutant dispersion (Saathoff et al. 1995; Meroney et al. 1999; Baker and Hargreaves 2001), wind-driven rain (Surry et al. 1994; Inculet 2001; Blocken and Carmeliet 2004), wind energy (Neff and Meroney 1998), wind loading on roofs and facades (Stathopoulos et al. 2002; Kumar et al. 2003; Chang and Meroney 2003; Kopp et al. 2005), wind effects on towers and bridges (McDonald et al. 2002; Gerges and Vickery 2003; Carril et al. 2003) and the stability of high-speed trains under cross wind (Baker et al. 2004).

Wind tunnel test section flow quality relates to temporal and spatial aspects of the flow. The amount of tolerable unsteadiness depends on the nature of the application and is subject of discussion in literature (Saric and Reshotko 1997; Reshotko and Saric 1998; Barlow et al. 1999). In this paper, only spatial aspects of the flow (uniformity, skewed flow and angularity) will be addressed. Strictly speaking, spatial uniformity is required in the entire empty test section of the wind tunnel: in each cross-section (i.e. in each plane perpendicular to the test section centre line) and in the streamwise direction (streamwise uniformity or horizontal homogeneity). The type of spatial uniformity required depends on the type of application. A distinction is made between aeronautical wind tunnels and atmospheric boundary layer wind tunnels. Aeronautical applications generally require a uniform flow field in the entire empty test section (Fig. 1a), while boundary layer wind tunnel studies, where the lower part of the atmospheric boundary layer has to be simulated, require "lateral" uniformity in the empty test section (Fig. 1b). Lateral uniformity implies that (1) the direction of the mean velocity vector is parallel to the test section centre line and (2) its magnitude is constant for each point along a horizontal line across the width of the test section. In the remainder of this paper we will limit the discussion to laterally uniform flows as required for Wind Engineering studies, but the presented methodology is applicable to entirely uniform flows as well.

Deviations from spatial uniformity can have negative repercussions on the test results (Rae and Pope 1984; Barlow et al. 1999). A skewed flow for example (i.e. with a streamwise velocity that is not

* Corresponding author: Peter Moonen, Laboratory of Building Physics, Department of Civil Engineering, K.U. Leuven, Kasteelpark Arenberg 40, 3001 Leuven, Belgium. Tel: + 32 (0) 16-321346 – Fax: + 32 (0) 16321980. E-mail address: peter.moonen@bwk.kuleuven.be

symmetrically distributed over the width of the test section) will cause the static pressure over the front face of an object placed in the test section and the position of the stagnation point to be shifted. This can have a significant influence on all measured quantities around the object.

Spatial flow uniformity is often documented by contour plots of velocity magnitude, static pressure or temperature that are shown in one or more cross-sectional planes of the wind tunnel (e.g. Selig and McGranahan, 2004). Other authors provide only numerical information in the form of a single mean value and spatial standard deviation for the quantity for the entire cross-sectional plane. The first method allows determining the presence or absence of skewness and angularity (up-flow, down-flow, cross-flow, etc.). However, multiple sections are required to obtain a complete view of the flow quality in the entire test section. Mean values and spatial standard deviations have the advantage that the flow in a specific (part of the) cross-section can be characterised numerically, although important information can be lost (e.g. the spatial standard deviation of the velocity magnitude in a cross section does not allow to distinguish between parabolic and skewed velocity profiles). The existing techniques do not allow for a complete and straightforward evaluation of test section flow quality. However, it is important to be able to quantify wind tunnel test section flow quality and to assess and compare the impact of features such as honeycombs, corner or guide vanes, screens, etc. for wind tunnel and flow quality optimisation.

In this paper, a set of six new complementary indices describing spatial uniformity and the different types of spatial non-uniformity is developed and they are applied to evaluate the test section flow quality of a closed-circuit wind tunnel. The flow fields are obtained by numerical simulations based on Computational Fluid Dynamics (CFD). In section 2, first some definitions are formulated. Next, the indicators for test section flow quality are introduced and their use is illustrated by a few straightforward examples (section 3). In section 4, the indices are used to evaluate the flow quality in the test section of a numerical closed-circuit wind tunnel and to assess the impact of adding guide vanes and a roughness screen upstream of the test section. Finally, the proposed approach is discussed and some general conclusions are formulated.

2. Definitions

In this section, a number of definitions are given that are used in the paper to characterise different features of the flow field.

Uniformity implies that the mean velocity vector only possesses a streamwise component with the same magnitude over the entire cross section (Fig. 2a). In reality, wall effects cause the velocity magnitude to decrease in the boundary layer near the walls. Generally this effect remains limited and we can still consider the flow field uniform (Fig. 2b). Several types of deviations from uniform flow can be distinguished. The two main categories are skewness and angularity. The flow exhibits skewness if the streamwise, lateral or vertical component of the mean wind velocity vector is not symmetrically distributed over the width of the test section (Fig. 2c). Angularity refers to mean velocity vectors at an angle to the test section centre line (Fig. 2d-e). Two types of angularity are defined. In the first type, the mean velocity vectors are parallel to each other but not to the test section centre line: the mean velocity vector possesses a lateral and/or a vertical component. If a lateral component is present, the term 'cross-flow' is often used (Fig. 2d). The vertical component is also termed 'up-flow' or 'down-flow' depending on the direction of the flow. In the second type, the stream lines are not parallel to each other and are symmetrically deviating from the test section centre line i.e. the flow is converging or diverging (Fig. 2e). In reality, both types will be simultaneously present.

3. Indicators for test section flow quality

This section describes the definitions of the new indices developed in this paper and their application to some simple theoretical examples.

3.1. Definitions

The definition of the indices is based on the fact that every function a(x) can be uniquely decomposed into a symmetric and an anti-symmetric function:

$$a(x) = b(x) + c(x) \tag{1}$$

where $b(x) = b(-x)$ is the symmetric part and $c(x) = -c(-x)$ is the anti-symmetric part. The differences between the ideal, uniform flow pattern and the actual flow pattern can be described in terms of symmetric and non-symmetric deviations (Fig. 2). E.g. wall friction causes a symmetric deviation, whereas skewness is non-symmetric; cross-flow is symmetric (the flow angle is the same at both sides of

the axis of the wind tunnel), whereas converging or diverging flows are non-symmetric (the flow angle is mirrored with respect to vertical centre plane of the wind tunnel). There are several ways to obtain the unique symmetric and anti-symmetric component of the mean velocity data. In this paper, the measurements at measurement points that are positioned symmetrically with respect to the vertical centre plane of the wind tunnel are compared. The average of the two data values yields the symmetric component. The difference between the average and the individual data values yields the anti-symmetric component.

Based on this knowledge, we can introduce 6 complementary indices, one of which describes lateral flow uniformity (2a) and fives others that describe different causes of lateral non-uniformity (2b-f):

$$I_{sym}^{U}(x,y)=\frac{\int U_{sym}^{2}(x,y,z)\,dz}{\int R^{2}(x,y,z)\,dz} \tag{2a}$$

$$I_{antisym}^{U}(x,y)=\frac{\int U_{antisym}^{2}(x,y,z)\,dz}{\int R^{2}(x,y,z)\,dz} \tag{2b}$$

$$I_{sym}^{V}(x,y)=\frac{\int V_{sym}^{2}(x,y,z)\,dz}{\int R^{2}(x,y,z)\,dz} \tag{2c}$$

$$I_{antisym}^{V}(x,y)=\frac{\int V_{antisym}^{2}(x,y,z)\,dz}{\int R^{2}(x,y,z)\,dz} \tag{2d}$$

$$I_{sym}^{W}(x,y)=\frac{\int W_{sym}^{2}(x,y,z)\,dz}{\int R^{2}(x,y,z)\,dz} \tag{2e}$$

$$I_{antisym}^{W}(x,y)=\frac{\int W_{antisym}^{2}(x,y,z)\,dz}{\int R^{2}(x,y,z)\,dz} \tag{2f}$$

where the integral is taken along a line across the width of the test section (Fig. 3); x, y and z are the streamwise, vertical and lateral coordinates; U, V and W are the streamwise, vertical and lateral components of the mean velocity vector in x, y and z-direction; and R is the velocity magnitude. The subscripts "sym" and "antisym" denote the symmetric and the anti-symmetric component respectively. By taking the square of each velocity component, the occurrence of imperfections like skewness or angularity is penalized and at the same time it is avoided that several anti-symmetric contributions cancel each other. The denominator normalizes the result to a value between zero and one.

I_{sym}^{U} is the index describing lateral flow uniformity. The definition is as such that the index equals one for uniform flow, even in the presence of symmetric deviations of the streamwise wind speed component (e.g. resulting from wall effects) since these imperfections cannot generally be avoided. The drawback of this approach will be discussed later in this paper. Imperfections in the flow field, like skewness and angularity, will lead to a lower value of the index of uniformity. The five other indices quantify these flow imperfections. Lower values correspond to better flow quality. $I_{antisym}^{U}$ is a measure for the skewness of the streamwise component of the flow. I_{sym}^{W} is related to cross-flow, $I_{antisym}^{W}$ to flow that is laterally converging or diverging. I_{sym}^{V} acts as a measure of up-flow or down-flow. $I_{antisym}^{V}$ indicates skewness in the vertical component of the flow. This quantity can to a certain extent be related to swirl.

Since $\int_{-a}^{+a} U_{sym}(x,y,z)\,U_{antisym}(x,y,z)\,dz=0$, with a an arbitrary positive real number, it can be shown that the sum of all indices equals 1 (Eq. 3).

$$I_{sym}^{U}+I_{antisym}^{U}+I_{sym}^{V}+I_{antisym}^{V}+I_{sym}^{W}+I_{antisym}^{W}=1 \tag{3}$$

or

$$I_{sym}^{U} = 1 - I_{antisym}^{U} - I_{sym}^{V} - I_{antisym}^{V} - I_{sym}^{W} - I_{antisym}^{W} \tag{4}$$

This relationship states that the index of uniformity I_{sym}^{U} equals one, reduced by all the contributions resulting from imperfections in the flow field. The index of uniformity acts as an indicator of flow quality. Good flow quality requires I_{sym}^{U} to be equal to one. Eq. (4) indicates that this can only be obtained if all other indices - related to imperfections in the flow field - are zero.

3.2. Examples

In this section, the indices are applied in some straightforward examples to illustrate their meaning. For simplicity, we will only consider velocity profiles along one horizontal line across the width of the test section. A more complex example will be given in section 4.

3.2.1. Uniform flow

In a uniform flow field, all streamlines are parallel to the centre plane of the wind tunnel and all velocity vectors have the same magnitude (Fig. 2a): Since the velocity distribution is symmetric with respect to the centre plane of the wind tunnel, the anti-symmetric components equal zero. As a result: $I_{sym}^{U} = 1$ and $I_{antisym}^{U} = I_{sym}^{V} = I_{antisym}^{V} = I_{sym}^{W} = I_{antisym}^{W} = 0$. In reality, friction near the wind-tunnel walls will prevent this ideal flow field (Fig. 2b). The effect is generally marginal. When the velocity profile remains symmetrically distributed the indices take the same value as in the case of ideal uniform flow.

3.2.2. Skewed flow

Consider the theoretical flow profile corresponding to Eq. 5 (Fig. 2c):

$$R = U = a_0 + a_1 z \tag{5}$$

where $z = 0$ corresponds to a point in the centre plane of the wind tunnel.
The symmetric and anti-symmetric components are:

$$U_{sym} = a_0 \quad ; \quad U_{antisym} = a_1 z \tag{6}$$

The index of uniformity becomes

$$I_{sym}^{U} = \frac{\int_{-B/2}^{+B/2} \left(a_0\right)^2 dz}{\int_{-B/2}^{+B/2} \left(a_0 + a_1 z\right)^2 dz} = \frac{3\left(2a_0\right)^2}{3\left(2a_0\right)^2 + \left(a_1 B\right)^2} \tag{7a}$$

and the other indices are given by:

$$I_{antisym}^{U} = \frac{\int_{-B/2}^{+B/2} \left(a_1 z\right)^2 dz}{\int_{-B/2}^{+B/2} \left(a_0 + a_1 z\right)^2 dz} = \frac{\left(a_1 B\right)^2}{3\left(2a_0\right)^2 + \left(a_1 B\right)^2} \tag{7b}$$

$$I_{sym}^{V} = I_{antisym}^{V} = I_{sym}^{W} = I_{antisym}^{W} = 0 \tag{7c}$$

In Eqs. (7a) and (7b), B is the total width of the test section. I_{sym}^{U} and $I_{antisym}^{U}$ can be non-zero in this situation, depending on the constants a_0 and a_1. The other indices are zero since there is no angularity in the flow field. If the symmetric component equals zero ($a_0 = 0$) the flow field is entirely skewed and the index $I_{antisym}^{U}$ equals one, independent of the value of a_1. If the average velocity in the test section is non-zero ($a_0 \neq 0$), $I_{antisym}^{U}$ tends asymptotically towards one with increasing skewness, whereas I_{sym}^{U} tends towards zero. Fig. 4 shows the evolution of I_{sym}^{U} and $I_{antisym}^{U}$ as a function of a_0 and $a_1 B$. Note that $I_{sym}^{U} + I_{antisym}^{U} = 1$, independent of the values of a_0 and a_1.

3.2.3. Cross-flow

Consider the theoretical flow profile corresponding to Eq. 8:

$$U = a_0$$
$$V = 0 \tag{8}$$
$$W = c_0 + c_1 z$$

where $z = 0$ corresponds to a point on the centre plane of the wind tunnel.
The symmetric and anti-symmetric components are:

$$U_{sym} = a_0$$
$$W_{sym} = c_0 \quad ; \quad W_{antisym} = c_1 z \tag{9}$$

The index of uniformity is given by:

$$I_{sym}^{U} = \frac{\int_{-B/2}^{+B/2} \left(a_0\right)^2 dz}{\int_{-B/2}^{+B/2} \left(a_0\right)^2 + \left(c_0 + c_1 z\right)^2 dz} = \frac{3\left(2a_0\right)^2}{3\left(2a_0\right)^2 + 3\left(2c_0\right)^2 + \left(c_1 B\right)^2} \tag{10a}$$

and the other indices are given by:

$$I_{sym}^{W} = \frac{\int_{-B/2}^{+B/2} \left(c_0\right)^2 dz}{\int_{-B/2}^{+B/2} \left(a_0\right)^2 + \left(c_0 + c_1 z\right)^2 dz} = \frac{3\left(2c_0\right)^2}{3\left(2a_0\right)^2 + 3\left(2c_0\right)^2 + \left(c_1 B\right)^2} \tag{10b}$$

$$I_{antisym}^{W} = \frac{\int_{-B/2}^{+B/2} \left(c_1 z\right)^2 dz}{\int_{-B/2}^{+B/2} \left(a_0\right)^2 + \left(c_0 + c_1 z\right)^2 dz} = \frac{\left(c_1 B\right)^2}{3\left(2a_0\right)^2 + 3\left(2c_0\right)^2 + \left(c_1 B\right)^2} \tag{10c}$$

$$I_{antisym}^{U} = I_{sym}^{V} = I_{antisym}^{V} = 0 \tag{10d}$$

First a velocity field with uniform lateral velocity as shown in Fig. 2d ($c_0 \neq 0$; $c_1 = 0$) is considered. In this case I_{sym}^{W} is nonzero and increases with increasing values of c_0, indicating that this index acts as a (relative) measure of flow angularity. Taking the arcsine of $\sqrt{I_{sym}^{W}}$ yields an approximate value of the average flow angle with the centre plane of the wind tunnel. Next, the situation with anti-symmetric lateral velocities as shown on Fig. 2e ($c_0 = 0$; $c_1 \neq 0$) is considered. This corresponds to a flow with converging or diverging flow lines. The magnitude of $I_{antisym}^{W}$ increases with increasing non-parallelism of the flow lines with respect to the centre plane of the wind tunnel. In both cases, the index of uniformity I_{sym}^{U} is smaller than one (Eq. 10a), indicating the lower flow quality. Fig. 5 shows the evolution of I_{sym}^{W} and $I_{antisym}^{W}$ as a function of c_0 and $c_1 B$. $I_{antisym}^{U}$, I_{sym}^{V} and $I_{antisym}^{V}$ remain zero, since there is no skewness and up-flow or down-flow are absent.

4. Application for a numerical closed-circuit wind tunnel

In this section, the indicators are applied to assess the impact of some geometrical features on the flow quality in the closed-circuit Jules Verne wind tunnel facility. First, the wind tunnel facility is briefly described, next the numerical simulation methodology is summarised and finally the influence of the presence of guide vanes and of a roughness screen on the flow quality in the test section is evaluated.

4.1. Wind tunnel facility

The configuration of the thermal circuit of the Jules Verne wind tunnel is shown in Fig. 6. Fig. 6a is the plan view. Fig. 6b and c are a longitudinal and a lateral cross-sectional view. Fig. 6d is a photograph of the nozzle, screen and guide vanes. The different sections of the wind tunnel are briefly described, starting from the test section and moving in the downstream direction. Numbers are used to refer to the

different features. A more detailed description of the tunnel can be found in Gandemer (1992) and in Moonen et al. (2006).
The test section (1) has a rectangular cross-sectional area of W x H = 10 x 7 m² and a length of 25 m. A sudden contraction (2) connects the downstream end of the test section to a 180° turn (3). The turn has a 6 x 7 m² rectangular cross-section at the outlet of the test section, which gradually widens to 7 x 7 m² at the fan-straightener section. Upstream of the fan there is an abrupt transition (4) from the rectangular to a circular cross-section (diameter 6.2 m) to take the flow into the fan. Flow straighteners (5) are present downstream of the fan blades to remove the swirl generated by the fan. Behind the fan-straightener section, there is a smooth transition of the cross section from circular back to rectangular (7 x 9 m²) by means of a small-angle diffuser (6). At the end of the diffuser, a heat exchanger is installed (7). The second 180° turn (8) gradually reduces the cross-sectional area to 6 x 9 m². At the end of the turn, two horizontal and six vertical guide vanes (9) are present to force the incident wind flow to be approximately parallel to the test section centre line and to increase the flow uniformity across the test section width. However, both measurements and numerical simulations show that the upper horizontal guide vane and the outer vertical vane generate a significant amount of turbulence in the test section (Moonen et al., 2006). Immediately downstream of the vanes, a screen (10) can be installed to generate vertical wind speed and turbulence intensity profiles that show a certain degree of similarity with those found in an atmospheric boundary layer (see Fig. 6c, d). Note that this screen is not a permanent feature of the wind tunnel. The adjustable nozzle (11) provides a contraction from the cross section at the end of the second turn (6 x 9 m²) to a cross-sectional area that can range from 6 x 5 m² to 6 x 3 m². This contraction is realized by suddenly lowering the height of the ceiling over a distance between 3 to 5 m and by raising the floor level by 1 m. Downstream of the contraction, a (very) short set of roughness elements is positioned (L x W = 4 x 6 m²), consisting of densely spaced cubes of 50 mm height (12). At the exit of the nozzle, the wind flow discharges into the larger test section (1).

4.2. Methodology

The approach developed by Moonen et al. (2006) is used to investigate numerically the influence of specific wind tunnel features on the test section flow quality. The authors showed that for this particular tunnel, it is required to model the entire wind tunnel to reliably reproduce the flow conditions of wind speed and turbulence intensity in the test section by means of CFD. The methodology was validated for the thermal circuit of the Jules Verne wind tunnel, both for the case of an empty wind tunnel and for the case in which a block-type building is placed in the test section. It consists in modeling the entire wind tunnel with sufficient detail (Fig. 7a). Earlier research has shown that it is not required to model the geometry of the fan-straightener section in detail and that it can be replaced by a fan boundary condition to which a pressure jump is applied. The particular choice for the pressure jump determines the operating point of the wind tunnel and hence the flow rate through and the pressure losses in the tunnel. Usually two calculations are needed. The first calculation uses an arbitrarily chosen value for the pressure jump and allows determining the system characteristic of the wind tunnel. Based on the knowledge of this characteristic and the desired operating point, the correct value for the pressure jump can be determined. This value is used for the actual calculation. This methodology is applied in combination with the indices presented in section 3 to study the impact of the guide vanes (subsection 4.3) and the roughness screen (subsection 4.4) on the flow quality in the test section.

For each configuration a different computational grid was generated. Suitable grids were obtained based on grid-sensitivity analyses and consisted of about 1.2 10^6 hexahedral cells. The majority of the cells was situated in the region surrounding the nozzle section. The three-dimensional Reynolds-Averaged Navier-Stokes (RANS) equations and the continuity equation were solved using the commercial CFD code Fluent 6.1 (Fluent Inc. 2006). Closure is obtained by using the realizable k-ε turbulence model (Shih et al. 1995). Near-wall modeling was performed using non-equilibrium wall functions (Kim and Choudhury, 1995). Pressure-velocity coupling was taken care of by the SIMPLEC algorithm (Vandoormaal and Raithby, 1984). Second order pressure interpolation was used. The QUICK discretization scheme was used for the convection terms of the governing equations and the equations of the turbulence model (Leonard, 1979).

4.3. Guide vanes

Four different configurations are investigated. The first one is the reference configuration in which no guide vanes are present. This configuration is compared to three others: with only horizontal vanes, only vertical vanes and a combination of horizontal and vertical vanes, respectively. The investigation of chord

length, curvature, orientation and other parameters determining the performance of the vanes is outside the scope of this paper. In all configurations, a roughness screen with blockage ratio of 8.5% is present in the nozzle (Fig. 6c, d). The blockage ratio is defined as the fraction of the cross-sectional area that is obstructed by the object.

4.3.1. Reference case: without guide vanes

Fig. 8a shows contours of the dimensionless velocity magnitude in a horizontal plane at 1.80 m height (left) and the vertical centre plane of the test section (right) for the case without guide vanes. The values are made dimensionless with respect to the streamwise wind speed at 2.1 m height at the inlet of the nozzle. Some remarks on the flow quality can be made. From the horizontal section, it can be seen that the velocity profile is not symmetric with respect to the vertical centre plane of the test section. The asymmetry results from the high curvature of the supply duct. It can be assumed that cross-flow is present, although this is not clear from Fig. 8a1. The vertical cross-section (Fig. 8a2) shows the increase of the velocity magnitude with height induced by installing the roughness screen. However it is seen that the velocity profile is not stable: it changes along the length of the test section. Given the geometry of the nozzle, a certain amount of up-flow and down-flow will be present.

The region that is studied by means of the flow quality indicators is indicated with a dotted line in Fig. 8b. Note that the sides and the top of the actual test section have been excluded from the analysis in order not to include the separations in these zones and to provide a fair picture of the flow quality. The index of uniformity I_{sym}^{U} is plotted in Fig. 9a as a percentage value. The flow quality is non-uniform: it decreases with increasing distance in the test section. Based on Fig. 8a1 one might arrive at the opposite conclusion. The apparent contradiction can be explained by the fact that wind profiles taken along the width of the test section show approximately the same skewness, but that the average velocity in the region of the analysis is higher at the inlet of the test section than at the outlet. As a result, the skewed velocity profile is less pronounced at the inlet, and hence flow quality is judged to be higher.

The five indices describing the deviations from uniform flow are applied to obtain a more detailed view of the test section flow quality. The intercomparison of the indices in Fig. 10 shows that skewness is most pronounced (up to 5%) whereas angularity (up-flow/down-flow, swirl, cross-flow, converging/diverging flow) is quite small (generally below 1%). Each index is analysed in more detail below.

Fig. 10a quantifies the skewness ($I_{antisym}^{U}$) of the velocity profile that was qualitatively indicated in Fig. 8a1. The index plot provides additional information because it can be seen that the relative skewness increases with increasing distance from the inlet of the test section and that the maximum relative skewness of the core flow is found at approximately 1.5 m height.

Fig. 10b quantifies up-flow or down-flow by means of I_{sym}^{V}. Although all values are quite low, the highest values are found in two regions. In the region in front of the inlet, this is related to the down-flow resulting from the specific nozzle geometry (the vertical reduction of the cross-section with 45%). The second region is situated at the top of the second half of the wind tunnel test section. This corresponds to up-flow, originating from the difference in height between the nozzle (5m) and the test section (7m).

The combination of Fig. 10c and d shows the presence of a limited amount of swirl in the flow field. Examination of the flow field confirmed that a spiral or helicoidal flow pattern develops in the bent flow channel. The presence of the roughness screen causes a decrease of the wind speed in the lower part of the tunnel, and shifts the core of the helicoidal flow upwards. $I_{antisym}^{V}$ reaches a maximum value at the position of the core of the helicoidal flow (±3m). The higher values of I_{sym}^{W} at about 2 m and 5 m height in the first part of the test section correspond respectively to the top and the bottom of the helicoidal flow.

Fig. 10e indicates lateral divergence or convergence ($I_{antisym}^{W}$). The test section can be roughly divided into two parts. In the first 16m of the test section, the wind flow is diverging due to the difference in width between the nozzle (6m) and the test section (10m). In the remaining part, the wind is converging again to enter the 180° turn leading towards the fan.

4.3.2. Horizontal, vertical or both types of guide vanes

Fig. 8b-d summarizes the CFD simulation results in terms of the dimensionless velocity magnitude. The calculations seem to indicate that adding the horizontal vanes has a slightly negative influence on the flow

pattern in the test section: the level of asymmetry increases a little bit and the jet at the top of the inlet is somewhat more pronounced. The white colour at this position indicates that the dimensionless wind speed reaches higher values than the maximum value on the colourbar (2.1). But the overall effect seems to remain limited (Fig. 8b). Adding vertical vanes (Fig. 8c) changes the appearance of the flow pattern: the velocity magnitudes become more symmetrically distributed over the width of the test section. It can be assumed that the angularity will be lower, but this can not be concluded from Fig. 8c. The combination of horizontal and vertical vanes (Fig. 8d) results in a flow pattern that seems to be less skewed in the first half of the test section and more skewed in the second half

Comparing the index of uniformity I_{sym}^{U} for the four different configurations (Fig. 9) reveals that adding horizontal guide vanes to the reference situation without vanes has a considerable negative impact (Fig. 9b): the flow quality decreases significantly. Adding the vertical vanes on the other hand has a very pronounced positive effect (Fig. 9c). This situation is slightly better than the combination of horizontal and vertical vanes (Fig. 9d).

A detailed view of the impact of the different configurations on the flow field in the test section can be obtained from the 5 indices describing flow imperfections. Comparing Fig. 10 and Fig. 11 reveals that the influence of horizontal guide vanes on test section flow quality is larger than the contours of velocity magnitude from Fig. 8 suggest. Especially the skewness increases (from 5 to 13%), whereas the other indices become only slightly higher. Contrary to what might be expected, the horizontal guide vanes in this wind tunnel do not suppress up-flow or down-flow (I_{sym}^{V}). These observations indicate that the vanes are too short and their intermediate distance is too large.

The positive influence of adding vertical guide vanes can be analysed by comparing Fig. 10 and Fig. 12. The contour plots of $I_{antisym}^{U}$ shows that the amount of skewness is significantly reduced (from 5 to 1%). Also, as expected, flow angularity is reduced, especially cross-flow (I_{sym}^{W}). Up-flow is still present in the upper half of the test section, but the situation has certainly improved (I_{sym}^{V}). Since the general lateral convergence/divergence of the flow-field is mainly determined by the difference in width between nozzle and test section width at the inlet, and between the width of the test section and of the bend towards the fan at the outlet, the influence on $I_{antisym}^{W}$ is limited.

The situation with horizontal and vertical guide vanes (Fig. 13) is slightly worse than in case only vertical guide vanes are present as was also indicated by Fig. 8.

4.4. Roughness screen

Three different configurations of the roughness screen are investigated: a configuration without screen and two configurations with screen, with an average blockage ratio of 8.5% and 12.5% respectively. The screens consist of wooden slats with dimensions 50 x 25 mm that span the entire nozzle width (Fig. 6c-d). The top bar reaches about 2 m above the ground of the test section. The number of bars is dependent on the desired blockage ratio and the spacing is linearly increasing with the height. Horizontal and vertical guide vanes are present in all calculations.

The roughness screen has the largest influence on the amount of skewness ($I_{antisym}^{W}$). Fig. 14 compares skewness maps for the three different screens. It is observed that an increase in blockage ratio causes a decrease in skewness from 2% to 1%. Note however that the intention of this screen was to generate vertical mean wind speed and turbulence profiles that are similar to those in the lower part of an atmospheric boundary layer, If it were a wire-mesh screen the influence on flow quality is expected to be much more pronounced.

5. Discussion

In this paper, the quality indicators were used in combination with CFD data. CFD provides data at every position in the numerical wind tunnel. They can also be used with experimental wind tunnel data, although this requires quite a large number of measurements at different locations in the test section.

In the definition of the index of uniformity, no differentiation is made between ‘uniform’ and ‘symmetric’ flow fields. This is motivated by the fact that wall effects are unavoidable and cause a symmetric deviation from the ideal uniform flow field. In general wall effects remain limited, and hence, the symmetric deviations do not adversely affect flow quality. However, in case these wall effects do not

remain limited or, more generally, in case arbitrary symmetric deviations occur, this is not detected by the index of uniformity. Although it could be stated that this type of non-uniformity is less likely to occur, the possibility should be born in mind when applying the indices. A possible way to detect symmetric deviations is to define an additional, variance-like quantity:

$$I_{sym}^{\Delta U}(x,y) = \frac{\int \left(U_{sym}(x,y,z) - \bar{U}_{sym}(x,y)\right)^2 dz}{\int R^2(x,y,z)\,dz} \tag{11}$$

where $\bar{U}_{sym}(x,y)$ is the average value of $U_{sym}(x,y,z)$ along a horizontal line across the width of the test section. For an entirely uniform flow field, $I_{sym}^{\Delta U}$ will be zero. Symmetric deviations like wall effects will result in a higher value of $I_{sym}^{\Delta U}$.

Besides the spatial variation of the velocity vector, also other quantities (e.g. turbulence intensity) can be investigated. For vector quantities it is sufficient to replace the velocity U by the quantity under investigation. For scalar quantities (e.g. temperature) the full set of indices reduces to two complementary indices.

The use of the indices is not restricted to the detection and quantification of lateral (non-)uniformity. By integrating over the height of the test section (dy) instead of the width (dz) in Eqs. 2a-f we obtain a new set of formulae that can be used in a horizontal cross-section (zx-plane). The combined information of quantities in a vertical and in a horizontal longitudinal cross-section gives information about the three dimensional skewness, angularity and the like.

The indices can be redefined by including a weighting or windowing function $w(x,y,z)$. For the index of uniformity (Eq. 2a), this yields

$$I_{sym}^{U}(x,y) = \frac{\int w(x,y,z)\,U_{sym}^2(x,y,z)\,dz}{\int w(x,y,z)\,R^2(x,y,z)\,dz} \tag{12}$$

The definitions of the other indices can be altered in the same way. The function $w(x,y,z)$ allows focussing on a specific region of interest by assigning higher weights to that region. If the same weighting function is used for all indices, it can be shown that Eqs. 3 and 4 still hold.

An important issue is the choice of threshold values for the different indices. Clearly, the index of uniformity should be as close to one as possible. Which level of imperfection can be tolerated depends on the application and is subject of further investigation.

6. Conclusions

A set of six new complementary indices for the evaluation of the spatial flow quality in wind tunnel test sections has been developed, presented and applied The first index quantifies spatial uniformity, while the other five indices are related to spatial imperfections in the flow field: skewness (one index) and flow angularity (indices for: up-flow/down-flow, swirl, cross-flow and converging/diverging flow).

The application of the indices to the thermal circuit of the Jules Verne wind tunnel indicated that they allow a detailed analysis of the flow quality in the test section. They can be visualized for the entire test section on a single graph and can provide useful information that can not directly be obtained from traditional velocity contour and vector plots or from numerical mean values and spatial standard deviations. In particular, the impact of adding guide vanes and a roughness screen in the nozzle was investigated. The indices showed that the vertical guide vanes reduce both skewness and angularity and therefore yield significantly higher flow quality. The current configuration of horizontal guide vanes was found to have a slightly negative impact.

The indices developed in this paper are applied in the design and optimization of the boundary layer wind tunnel of the Laboratory of Building Physics, K.U.Leuven. The authors hope that the indices will also be found useful in the evaluation and optimization of test-section flow quality in other wind tunnels.

Acknowledgements

The second author is a post-doctoral fellow of the FWO-Flanders (Research Fund-Flanders) that supports fundamental research in Flanders, Belgium. Their financial support is gratefully acknowledged.

References

Baker, C.J., Hargreaves, D.M., 2001. Wind tunnel evaluation of a vehicle pollution dispersion model. Journal of Wind Engineering and Industrial Aerodynamics, 89, 2, 187-200.

Baker, C.J., Jones, J., Lopez-Calleja, F., Munday, J. 2004. Measurements of the cross wind forces on trains. Journal of Wind Engineering and Industrial Aerodynamics 92, 7-8, 547-563.

Barlow, J.B., Rae, W.H., Pope, A., 1999. Low-speed wind tunnel testing. Third Edition, John Wiley & Sons.

Blocken, B., Carmeliet, J., 2004. A review of wind-driven rain research in building science. Journal of Wind Engineering and Industrial Aerodynamics 92, 13, 1079-1130.

Carril, C.F., Isyumov, N., Brasil, R., 2003. Experimental study of the wind forces on rectangular latticed communication towers with antennas. Journal of Wind Engineering and Industrial Aerodynamics 91, 8, 1007-1022.

Chang, C.H., Meroney, R.N., 2003. The effect of surroundings with different separation distances on surface pressures on low-rise buildings. Journal of Wind Engineering and Industrial Aerodynamics 91, 8, 1039-1050.

Fluent Inc., 2003. Fluent 6.1 User's Guide. Lebanon, New Hampshire.

Gandemer, J., 1992. La soufflerie climatique "Jules Verne". Journal of Wind Engineering and Industrial Aerodynamics 41-44, 43-54.

Gerges, R.R., Vickery, B.J., 2003. Wind tunnel study of the across-wind response of a slender tower with a nonlinear tuned mass damper. Journal of Wind Engineering and Industrial Aerodynamics 91, 8, 1069-1092.

Inculet, D.R., 2001. The design of cladding against wind-driven rain. Ph.D. thesis, The University of Western Ontario, London, Canada, 297 p.

Kim, S.-E., Choudhury, D., 1995. A near-wall treatment using wall functions sensitized to pressure gradient. ASME FED 217, 273-280.

Kopp, G.A., Surry, D., Mans, C., 2005. Wind effects of parapets on low buildings: Part 1. Basic aerodynamics and local loads. Journal of Wind Engineering and Industrial Aerodynamics, 93, 11, 817-841.

Kumar, K.S., Stathopoulos, T., Wisse, J.A., 2003. Field measurement data of wind loads on rainscreen walls. Journal of Wind Engineering and Industrial Aerodynamics 91, 11, 1401-1417.

Leonard, B.P., 1979. A Stable and Accurate Convection Modeling Procedure Based on Quadratic Upstream Interpolation. Computer Methods in Applied Mechanics and Engineering 19, 59-98.

Macdonald, J.H.G., Irwin, P.A., Fletcher, M.S, 2002. Vortex-induced vibrations of the Second Severn Crossing cable-stayed bridge: full-scale and wind tunnel measurements. Proceedings of the Institution of Civil Engineers - Structures and Buildings 152 (2): 123-134.

Meroney, R.N., Leitl, B.M., Rafailidis, S., Schatzmann, M., 1999. Wind-tunnel and numerical modeling of flow and dispersion about several building shapes. Journal of Wind Engineering and Industrial Aerodynamics 81, 333-345.

Moonen, P., Blocken, B., Roels, S., Carmeliet, J. Numerical modeling of the flow conditions in a closed-circuit low-speed wind tunnel. Journal of Wind Engineering and Industrial Aerodynamics. In press.

Neff, D.E., Meroney, R.N., 1998. Wind-tunnel modeling of hill and vegetation influence on wind power availability. Journal of Wind Engineering and Industrial Aerodynamics, 74-76, 335-343.

Rae (jr.), W.H., Pope, A., 1984. Low-speed wind tunnel testing. John Wiley and Sons, New York.

Reshotko, E., Saric, W.S., Nagib, H.M., 1998. Review of flow quality issues in wind tunnel testing, AIAA-1998-2613.

Richards, P.J., Mallinson, G.D., McMillan, D., Li, Y.F., 2002. Pedestrian level wind speeds in downtown Auckland. Wind and Structures 5, 2-4, 151-164.

Saathoff, P.J., Stathopoulos, T., Dobrescu, M., 1995. Effects of model scale in estimating pollutant dispersion near buildings. Journal of Wind Engineering and Industrial Aerodynamics 54, Issue contributed to Third Asian-Pacific Symposium on Wind Engineering, 549-559.

Saric, W.S., Reshotko, E., 1997. Review of flow quality issues for large wind tunnels. AIAA Aerospace Sciences Meeting & Exhibit, 35th, Reno, NV, Jan 6-9, 1997.

Selig, M.S., McGranahan, B.D., 2004. Wind tunnel aerodynamic tests of six airfoils for use on small wind turbines, AIAA-2004-1188.

Shih, T.-H., Liou, W.W., Shabbir, A., Yang, Z., Zhu, J., 1995. A new k-ε eddy viscosity model for high Reynolds number turbulent flows. Computers & Fluids 24, 227-238.

Stathopoulos, T., Saathoff, P., Du, X., 2002. Wind loads on parapets. Journal of Wind Engineering and Industrial Aerodynamics, 90, 4-5, 503-514.

Sundare Murthy, H., Verma, R.S., Jagadeeswrachar, S.P., Kumar, R., 2001. Flow Quality improvements in a blowdown wind tunnel. Journal of Aircraft 38, 577-580.

Surry, D., Inculet, D.R., Skerlj, P.F., Lin, J.X., Davenport, A.G., 1994. Wind, rain and the building envelope – a status report of ongoing research at the University of Western Ontario. Journal of Wind Engineering and Industrial Aerodynamics 53, 1-2, 19-36.

Vandoormaal, P., Raithby, G. D., 1984. Enhancements of the SIMPLE Method for Predicting Incompressible Fluid Flows. Numerical Heat Transfer 7, 147-163.

Wu, H.Q., Stathopoulos, T., 1993. Wind tunnel techniques for assessment of pedestrian-level winds. Journal of Engineering Mechanics – ASCE 119, 10, 1920-1936.

Symbol list

B	Total width of the test section	m
G_a	Volumetric flow rate	m^3/s
k	Turbulent kinetic energy	m^2/s^2
R	Magnitude of the mean velocity vector	m/s
U,V,W	Average mean velocity components in streamwise, vertical and lateral direction	m/s
w	Windowing or weighting function	-
x, y, z	Streamwise, vertical and lateral Cartesian co-ordinates	m
ε	Turbulence dissipation rate	m^2/s^3

Figure captions

Fig. 1: Required flow fields in wind tunnel test sections: (a) entirely uniform flow for aeronautical applications and (b) laterally uniform flow for Wind Engineering studies.

Fig. 2: Top row: Definition of different types of flow: (a) ideal uniform flow; (b) symmetric flow resulting from wall friction; (c) skewed flow; (d) angularity (cross-flow or up-flow); (e) angularity (diverging or converging flow). Situations (c), (d) and (e) are to be avoided. Second and third row: decomposition of the original flow field into a symmetric and an anti-symmetric component.

Fig. 3: A component of the mean velocity vector is integrated along a horizontal line across the width of the test section to obtain a value for the corresponding index. In this way, the quality of the three dimensional flow in the test section can be shown on a two-dimensional graph.

Fig. 4: Dependency of $I^{U}_{antisym}$ (left) and I^{U}_{sym} (right) on the characteristics of a linear flow field. a_0 is the average wind speed over in the cross-section, $a_1 B$ determines the amount of skewness.

Fig. 5: Dependency of $I^{W}_{antisym}$ (left) and I^{W}_{sym} (right) on the characteristics of a linear flow field. c_0 is the average wind speed over in the cross-section, $c_1 B$ determines the amount of skewness.

Fig. 6: a) Plan view, (b) longitudinal cross-sectional view, (c) lateral cross-sectional view and (d) photograph of nozzle, screen and guide vanes of the thermal circuit of the Jules Verne wind tunnel facility. The different sections and features of the wind tunnel are indicated with numbers. All dimensions are given in meter.

Fig. 7: (a) Geometrical model of the Jules Verne wind tunnel facility used for the CFD simulations; (b) Computational mesh at the surface of the guide vanes and screen; (c) Geometry of the guide vanes (horizontal cross section); (d) Mesh around the guide vanes (horizontal cross section).

Fig. 8: Contours of dimensionless velocity magnitude in a horizontal plane at 1.80 m height (left) and in the vertical centre plane which of the test section (right) for 4 different situations: (a) no vanes; (b) only horizontal vanes; (c) only vertical vanes and (d) horizontal and vertical vanes. The region that is studied by means of the flow quality indicators is indicated with a dotted line in Fig. b. Dimensionless wind speeds higher than 2.1 are coloured white (see top of nozzle).

Fig. 9: Contour plots of the uniformity index I^{U}_{sym} for 4 different situations: (a) no vanes; (b) only horizontal vanes; (c) only vertical vanes and (d) horizontal and vertical vanes. The index is given in a vertical plane parallel to the test section centre plane The coordinate system is depicted in Fig. 6.

Fig. 10: Contour plots of 5 flow-quality indicators for the configuration without guide vanes. They are given in a vertical plane parallel to the test-section centre plane: (a) $I^{U}_{antisym}$ (skewness); (b) I^{V}_{sym} (up-flow or down-flow); (c) $I^{V}_{antisym}$ (swirl); (d) I^{W}_{sym} (cross-flow); (e) $I^{W}_{antisym}$ (converging or diverging flow). The coordinate system is depicted in Fig. 6.

Fig. 11: Contour plots of 5 flow-quality indicators for the configuration with only horizontal guide vanes. They are given in a vertical plane parallel to the test-section centre plane: (a) $I^{U}_{antisym}$ (skewness); (b) I^{V}_{sym} (up-flow or down-flow); (c) $I^{V}_{antisym}$ (swirl); (d) I^{W}_{sym} (cross-flow); (e) $I^{W}_{antisym}$ (converging or diverging flow). The coordinate system is depicted in Fig. 6.

Fig. 12: Contour plots of 5 flow-quality indicators for the configuration with only vertical guide vanes. They are given in a vertical plane parallel to the test-section centre plane: (a) $I^{U}_{antisym}$ (skewness); (b) I^{V}_{sym} (up-flow or down-flow); (c) $I^{V}_{antisym}$ (swirl); (d) I^{W}_{sym} (cross-flow); (e) $I^{W}_{antisym}$ (converging or diverging flow). The coordinate system is depicted in Fig. 6.

Fig. 13: Contour plots of 5 flow-quality indicators for the configuration with horizontal and vertical guide vanes. They are given in a vertical plane parallel to the test-section centre plane: (a) $I^{U}_{antisym}$ (skewness); (b) I^{V}_{sym} (up-flow or down-flow); (c) $I^{V}_{antisym}$ (swirl); (d) I^{W}_{sym} (cross-flow); (e) $I^{W}_{antisym}$ (converging or diverging flow). The coordinate system is depicted in Fig. 6.

Fig. 14: Contour plots of $I^{U}_{antisym}$ in a vertical plane parallel to the centre plane of the test-section for roughness screens with a blockage ratio of (a) 0%, (b) 8.5% or (c) 12.5%. The coordinate system is depicted in Fig. 6.

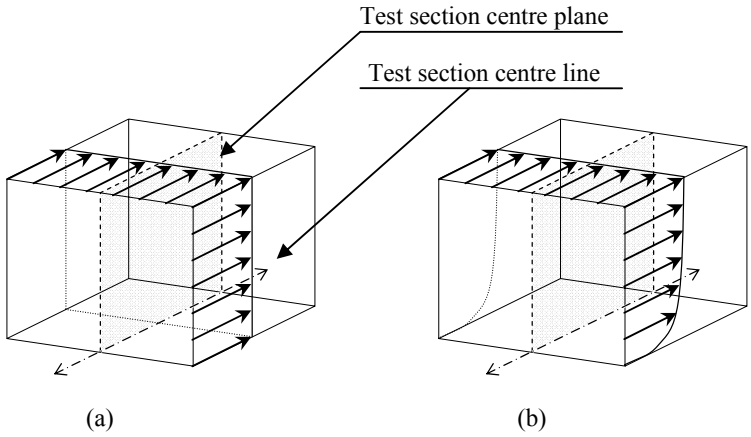

Figure 1

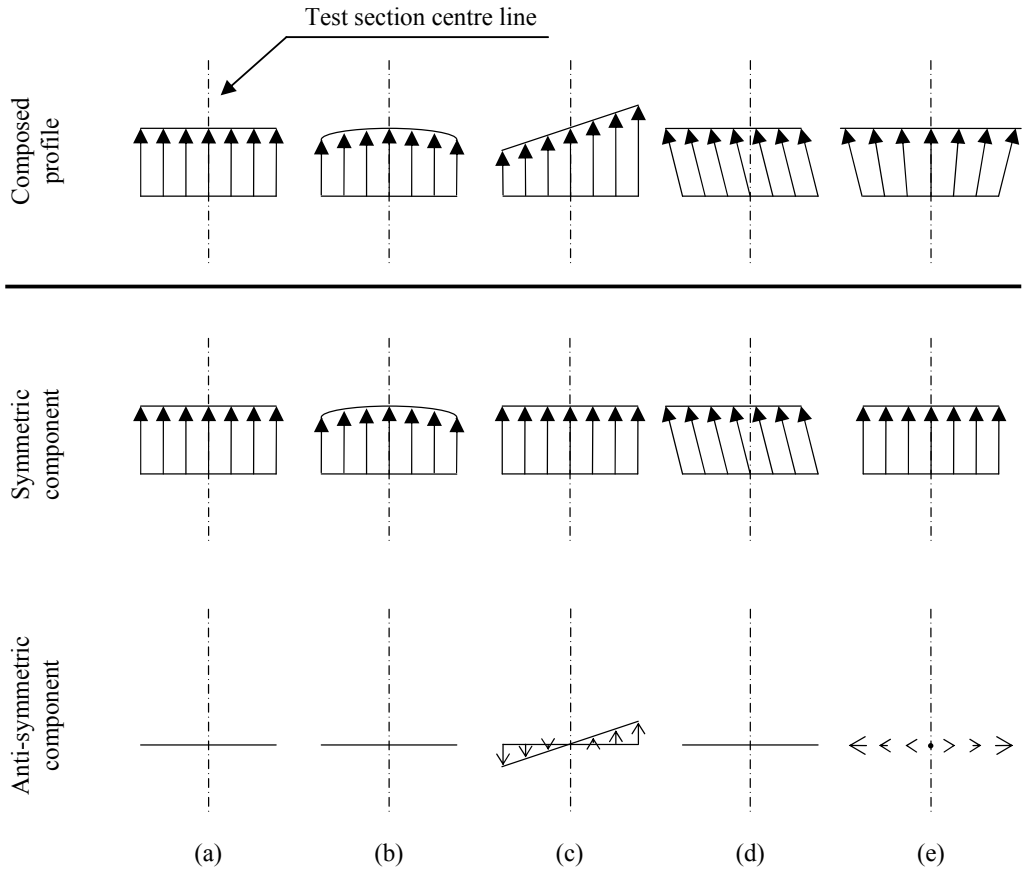
Test section centre line
Composed profile
Symmetric component
Anti-symmetric component
(a)
(b)
(c)
(d)
(e)

Figure 2

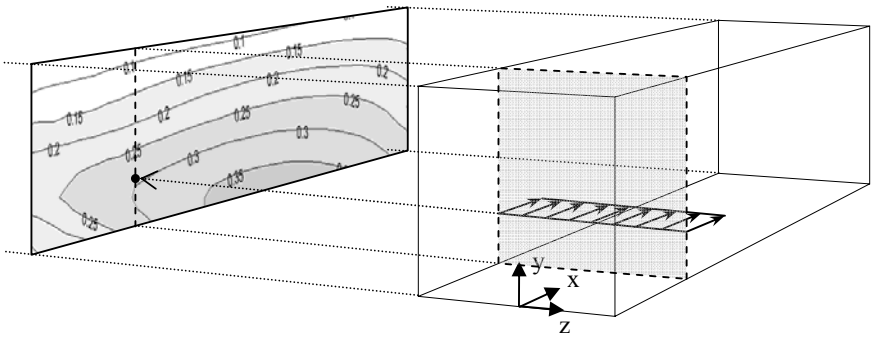

2D-graph 3D test section

Figure 3

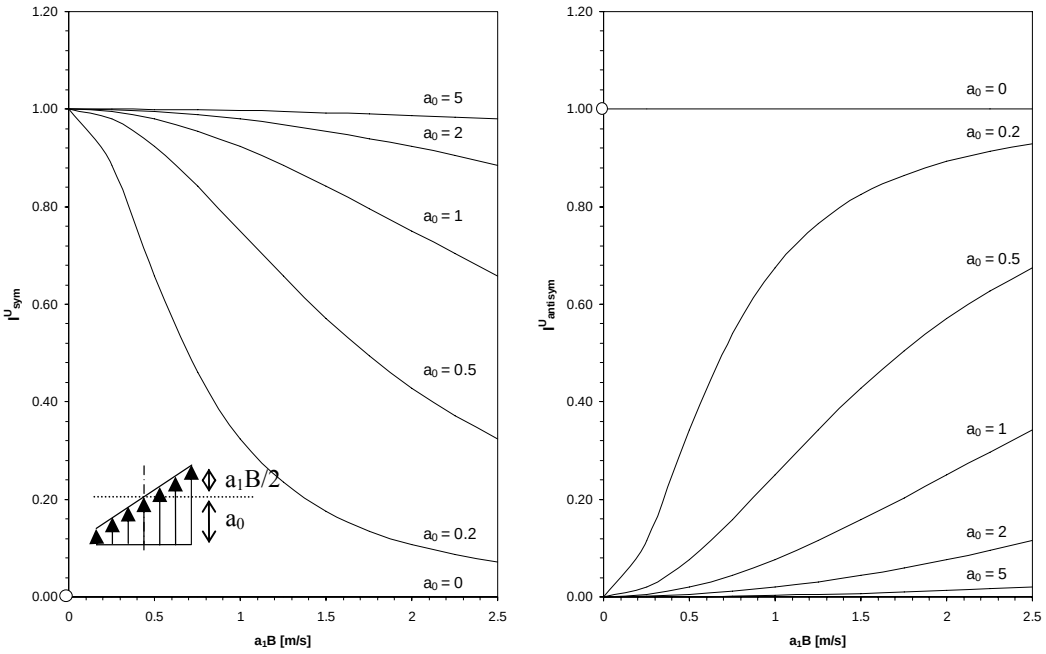
1.20
1.00
0.80
0.60
0.40
0.20
0.00
I^{U}_{sym}
$a_0 = 5$
$a_0 = 2$
$a_0 = 1$
$a_0 = 0.5$
$a_0 = 0.2$
$a_0 = 0$
$a_1B/2$
a_0
0
0.5
1
1.5
2
2.5
a_1B [m/s]
$I^{U}_{antisym}$
$a_0 = 0$
$a_0 = 0.2$
$a_0 = 0.5$
$a_0 = 1$
$a_0 = 2$
$a_0 = 5$

Figure 4

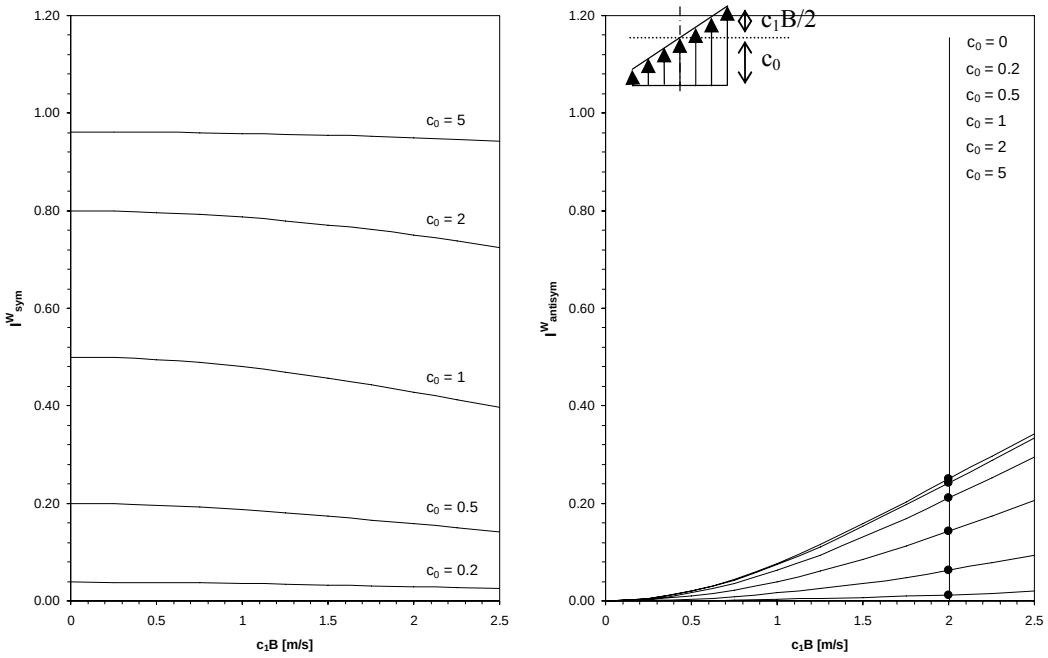
1.20
1.00
0.80
0.60
0.40
0.20
0.00
0
0.5
1
1.5
2
2.5
c_1B [m/s]
I^W_{sym}
c_0 = 5
c_0 = 2
c_0 = 1
c_0 = 0.5
c_0 = 0.2
$I^W_{antisym}$
$c_1B/2$
c_0
c_0 = 0
c_0 = 0.2
c_0 = 0.5
c_0 = 1
c_0 = 2
c_0 = 5

Figure 5

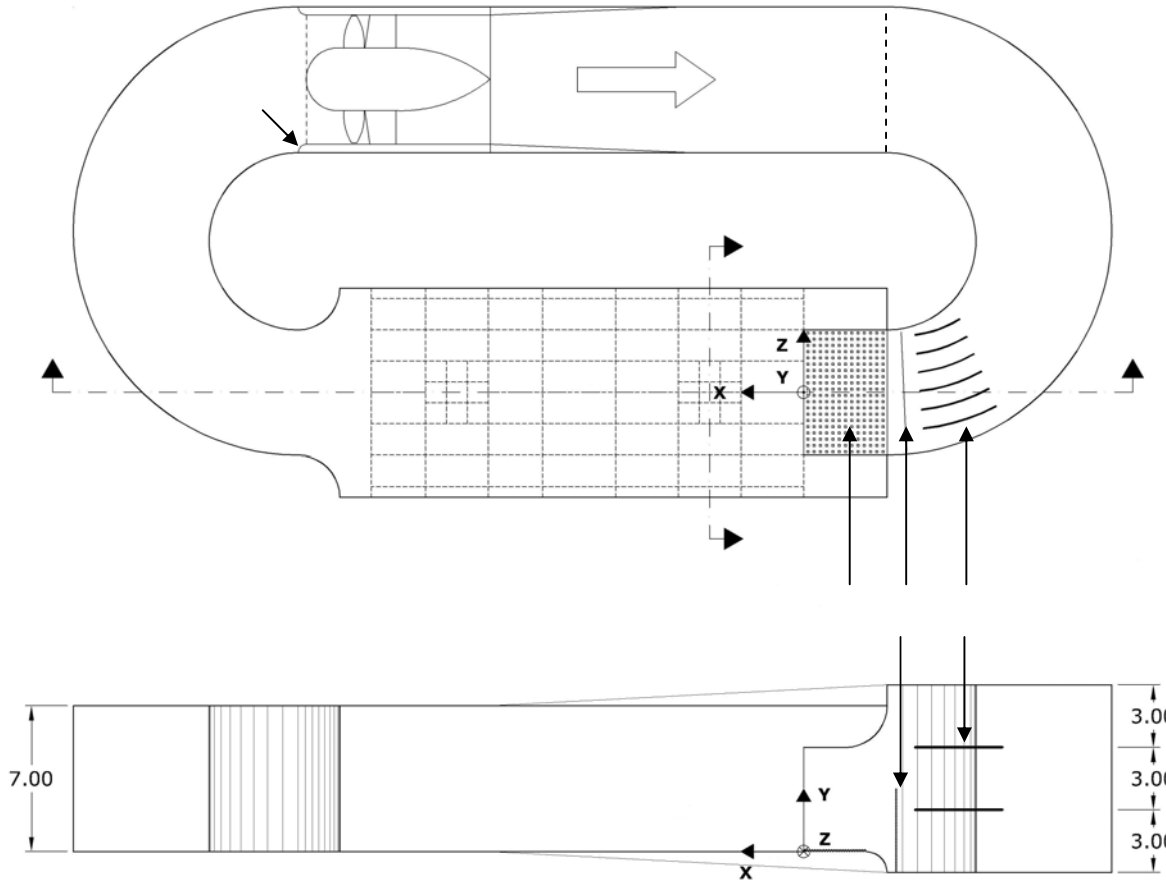
Z
Y
X
7.00
3.00
3.00
3.00
Y
Z
X

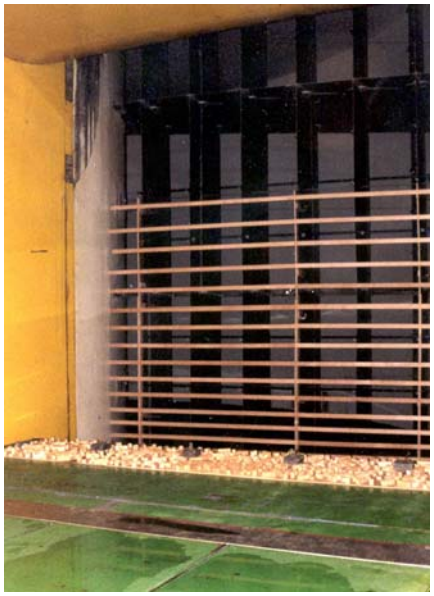

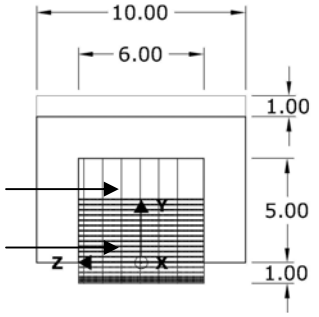
10.00
6.00
1.00
5.00
1.00
Y
Z
X

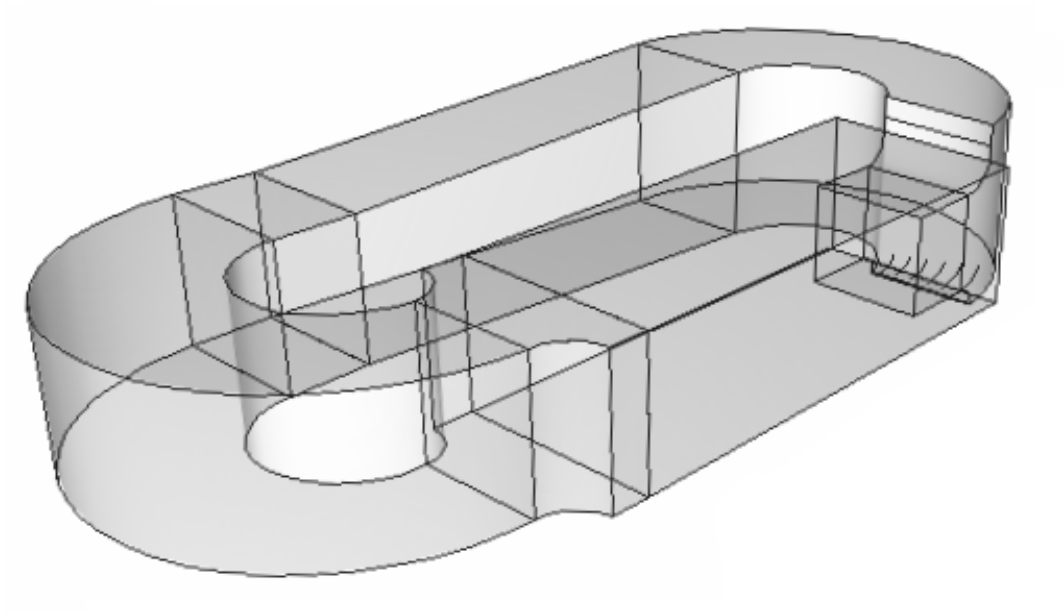

(a)

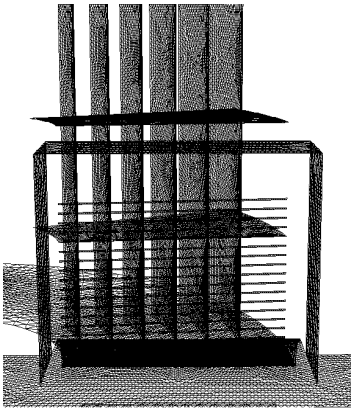

(b)

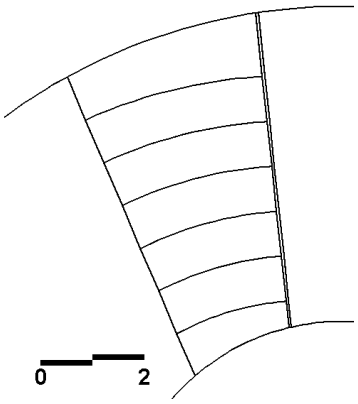

(c)

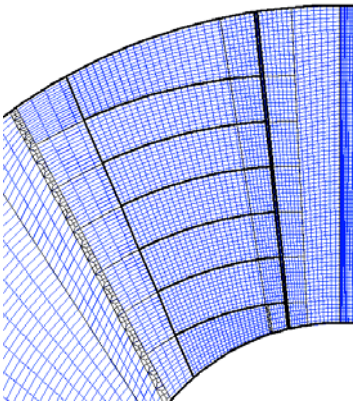

(d)

Figure 7

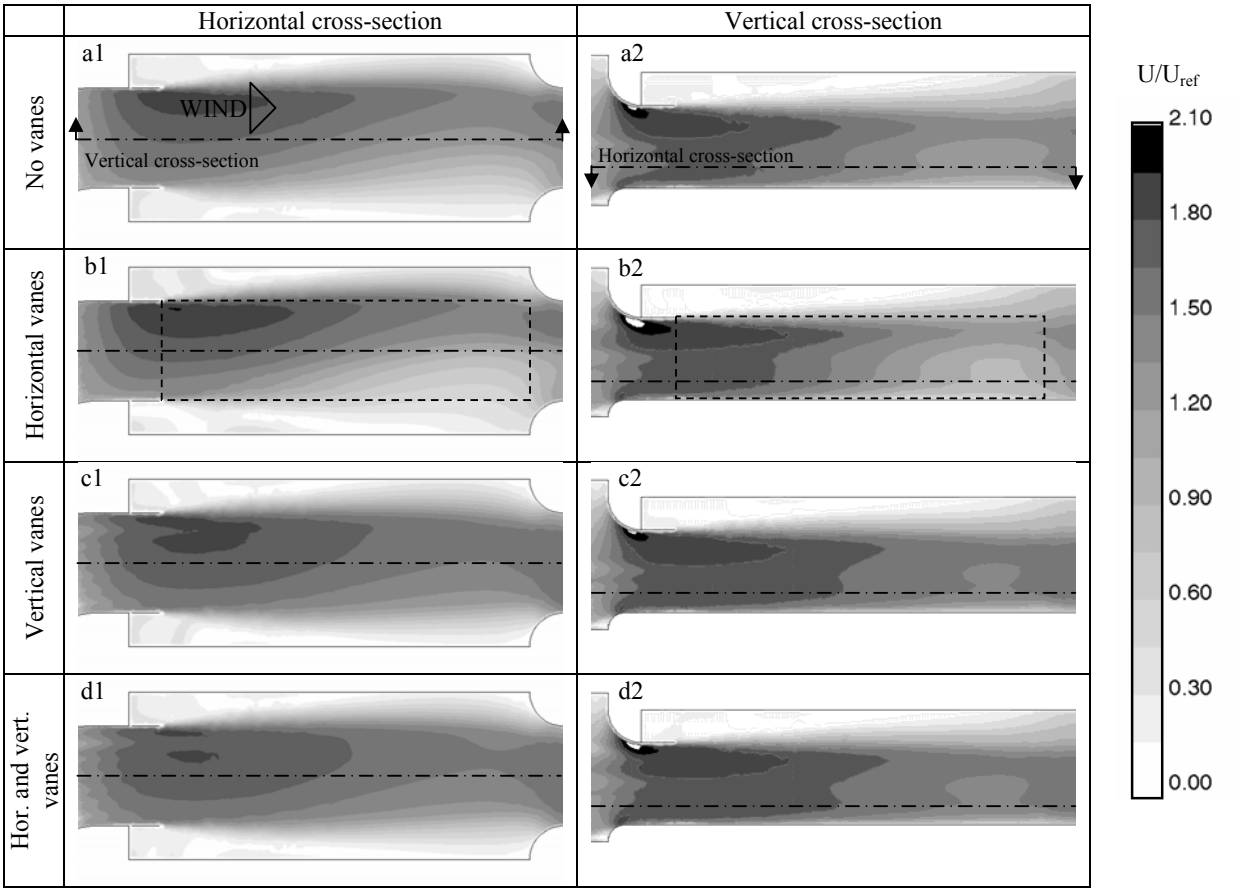
Horizontal cross-section
Vertical cross-section
No vanes
Horizontal vanes
Vertical vanes
Hor. and vert. vanes
a1
WIND
Vertical cross-section
a2
Horizontal cross-section
b1
b2
c1
c2
d1
d2
U/U_ref
2.10
1.80
1.50
1.20
0.90
0.60
0.30
0.00

Figure 8

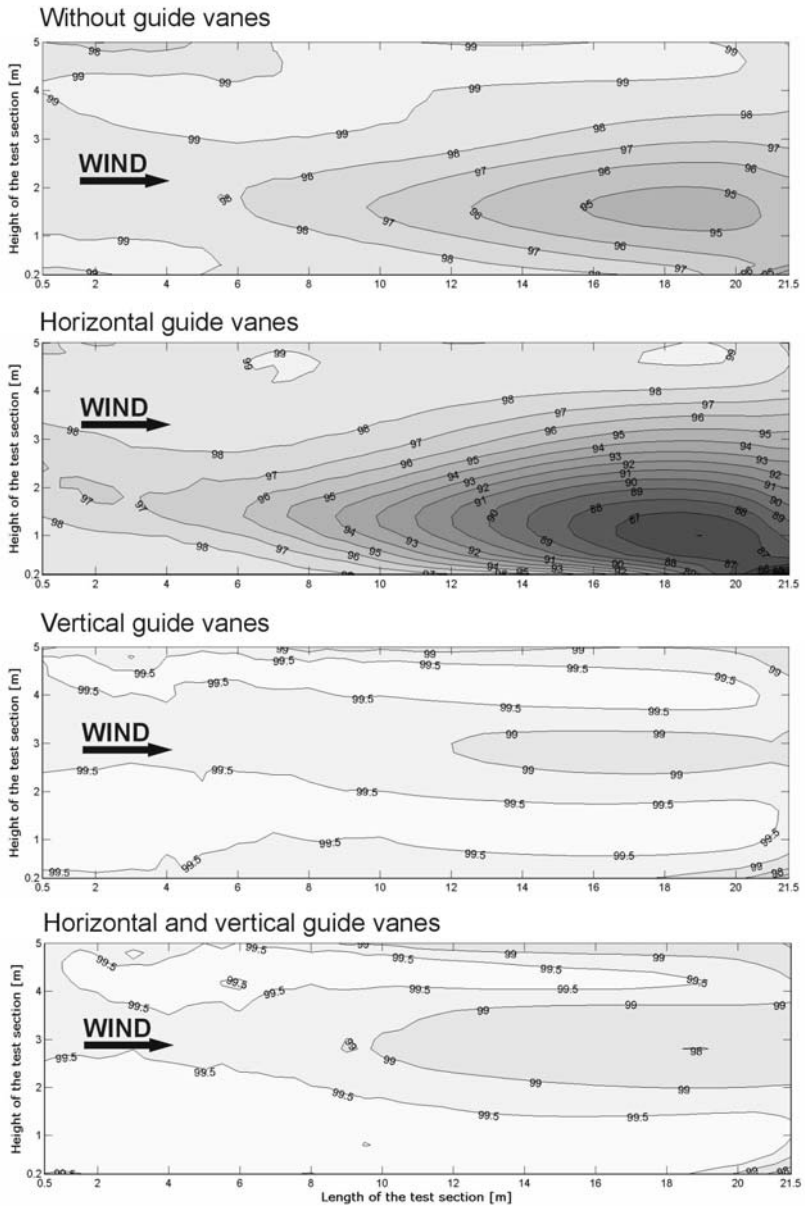
INDEX OF UNIFORMITY (I^{u}_{sym})
Without guide vanes
Horizontal guide vanes
Vertical guide vanes
Horizontal and vertical guide vanes
WIND
Height of the test section [m]
Length of the test section [m]

Figure 9

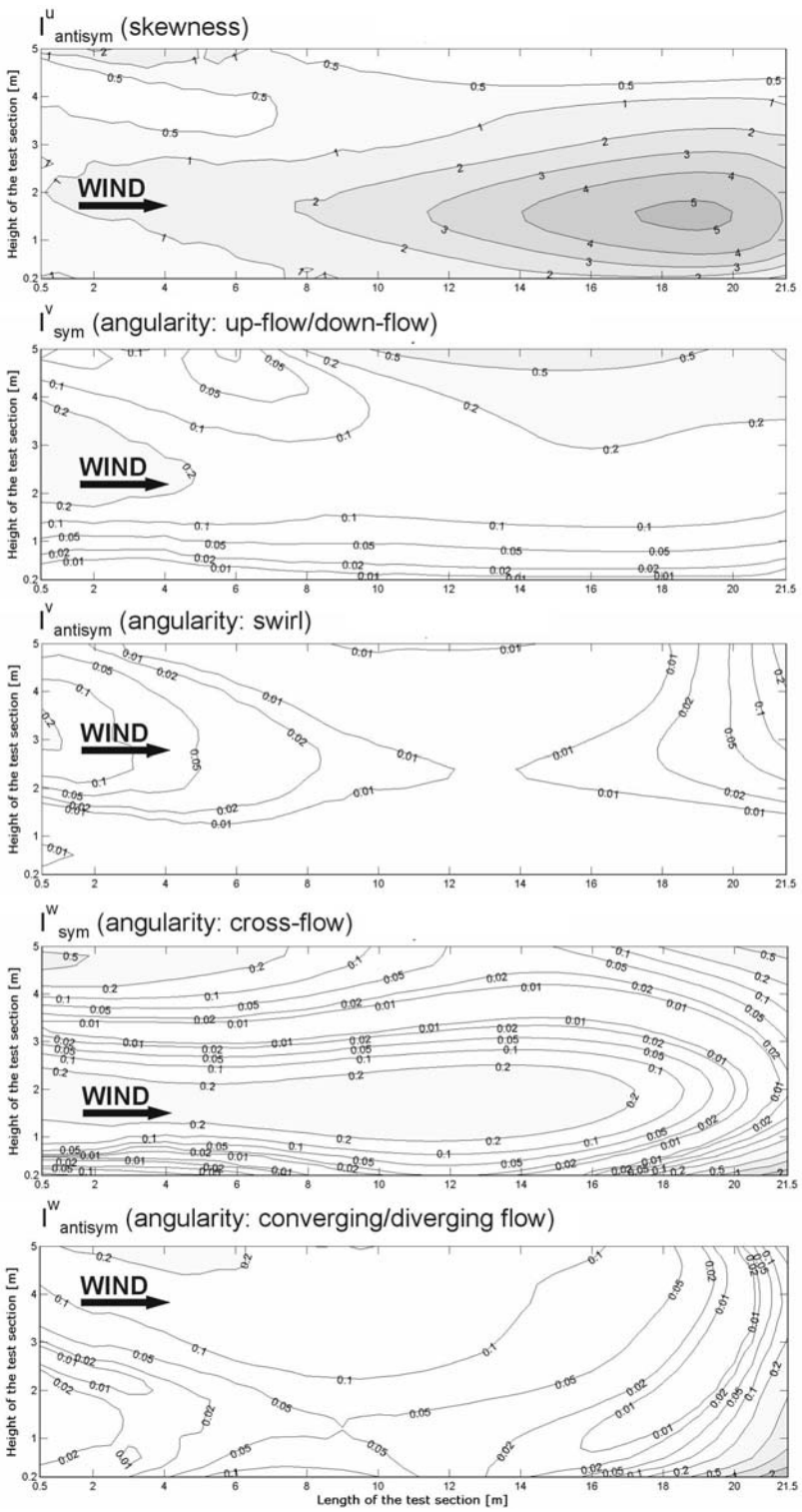
WITHOUT GUIDE VANES
I u antisym (skewness)
I v sym (angularity: up-flow/down-flow)
I v antisym (angularity: swirl)
I w sym (angularity: cross-flow)
I w antisym (angularity: converging/diverging flow)
WIND
Height of the test section [m]
Length of the test section [m]

Figure 10

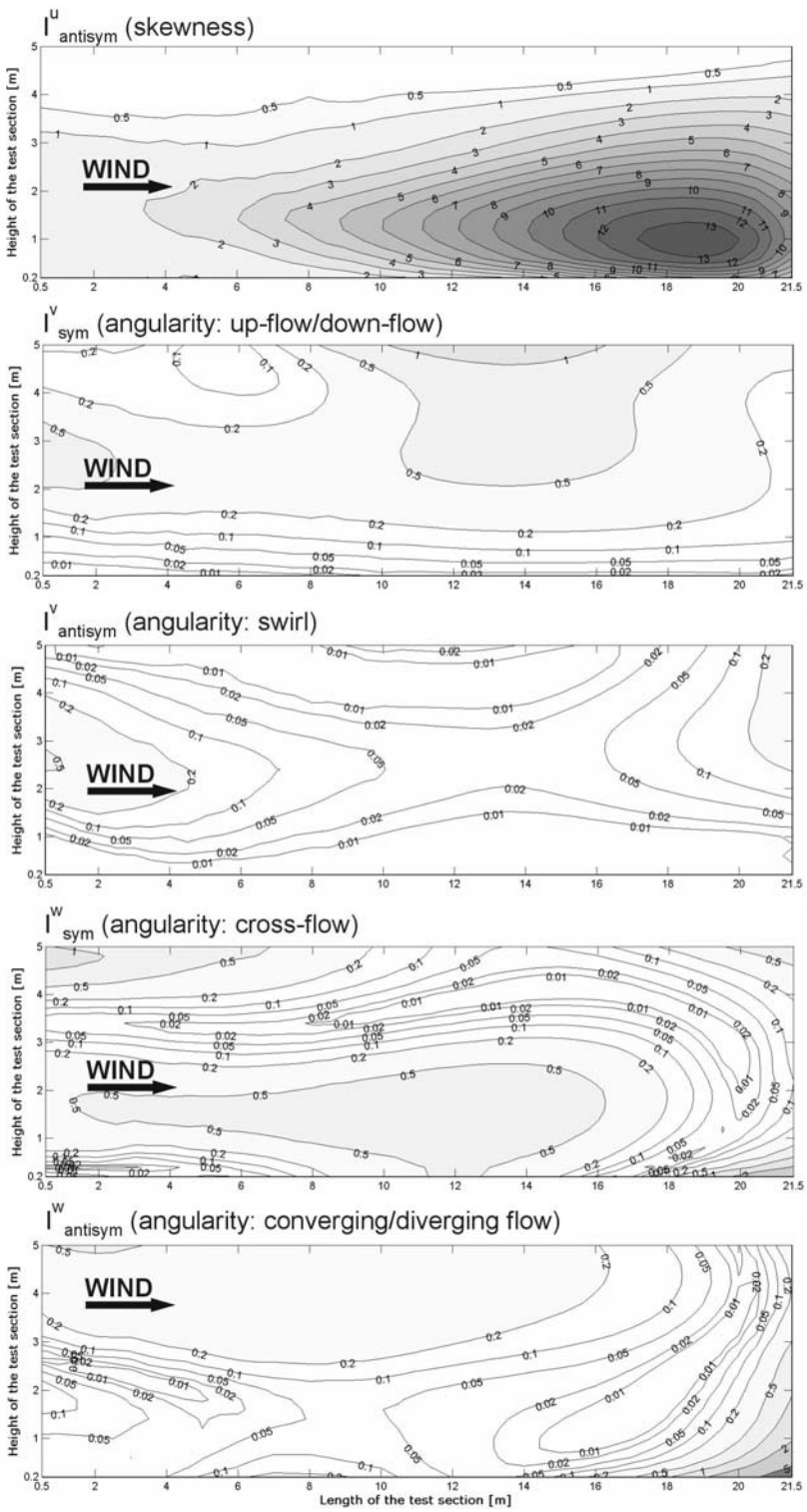
HORIZONTAL GUIDE VANES
$I^{u}_{antisym}$ (skewness)
I^{v}_{sym} (angularity: up-flow/down-flow)
$I^{v}_{antisym}$ (angularity: swirl)
I^{w}_{sym} (angularity: cross-flow)
$I^{w}_{antisym}$ (angularity: converging/diverging flow)
WIND
Height of the test section [m]
Length of the test section [m]

Figure 11

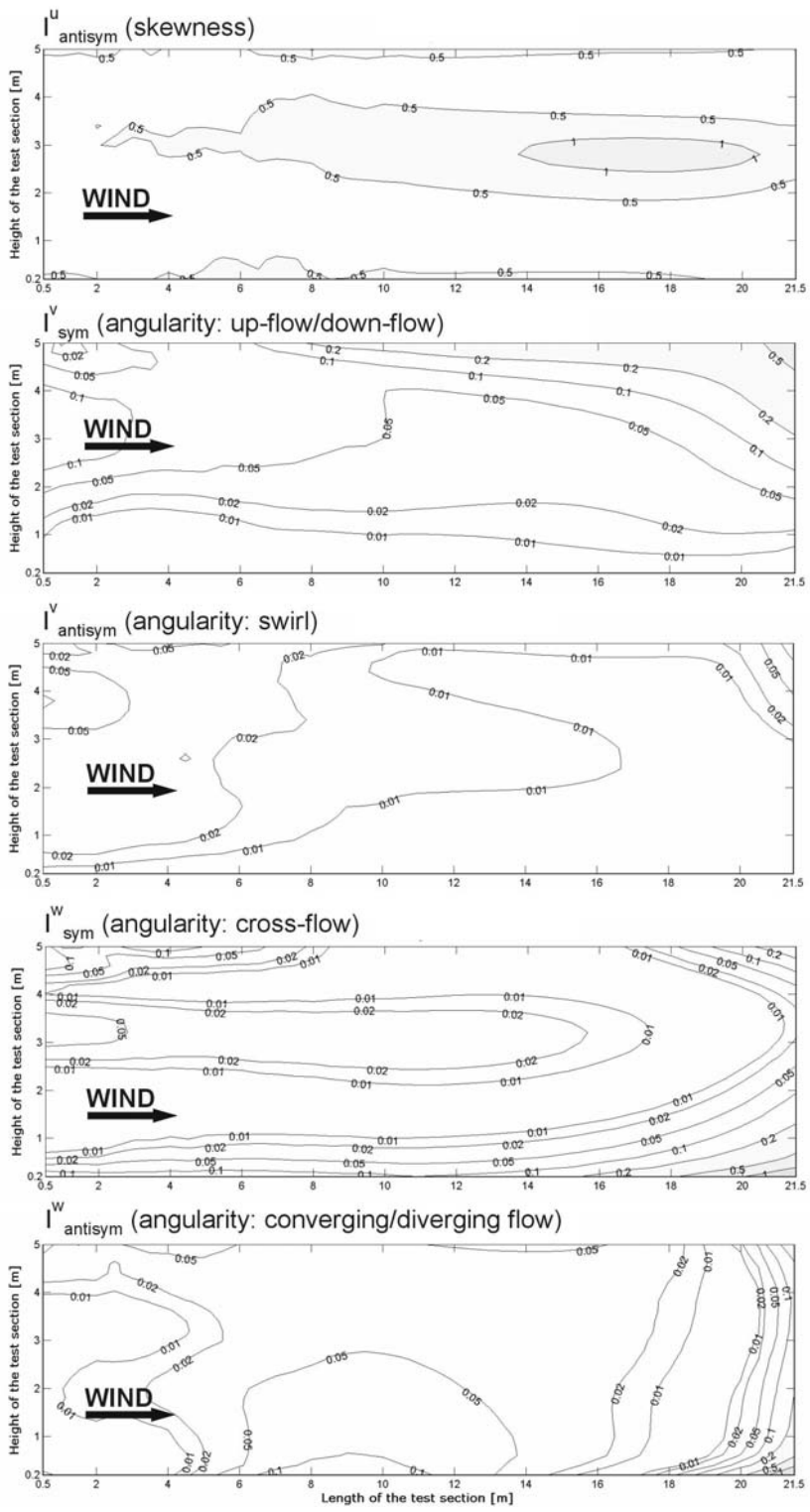
VERTICAL GUIDE VANES
I u antisym (skewness)
I v sym (angularity: up-flow/down-flow)
I v antisym (angularity: swirl)
I w sym (angularity: cross-flow)
I w antisym (angularity: converging/diverging flow)
WIND
Height of the test section [m]
Length of the test section [m]

Figure 12

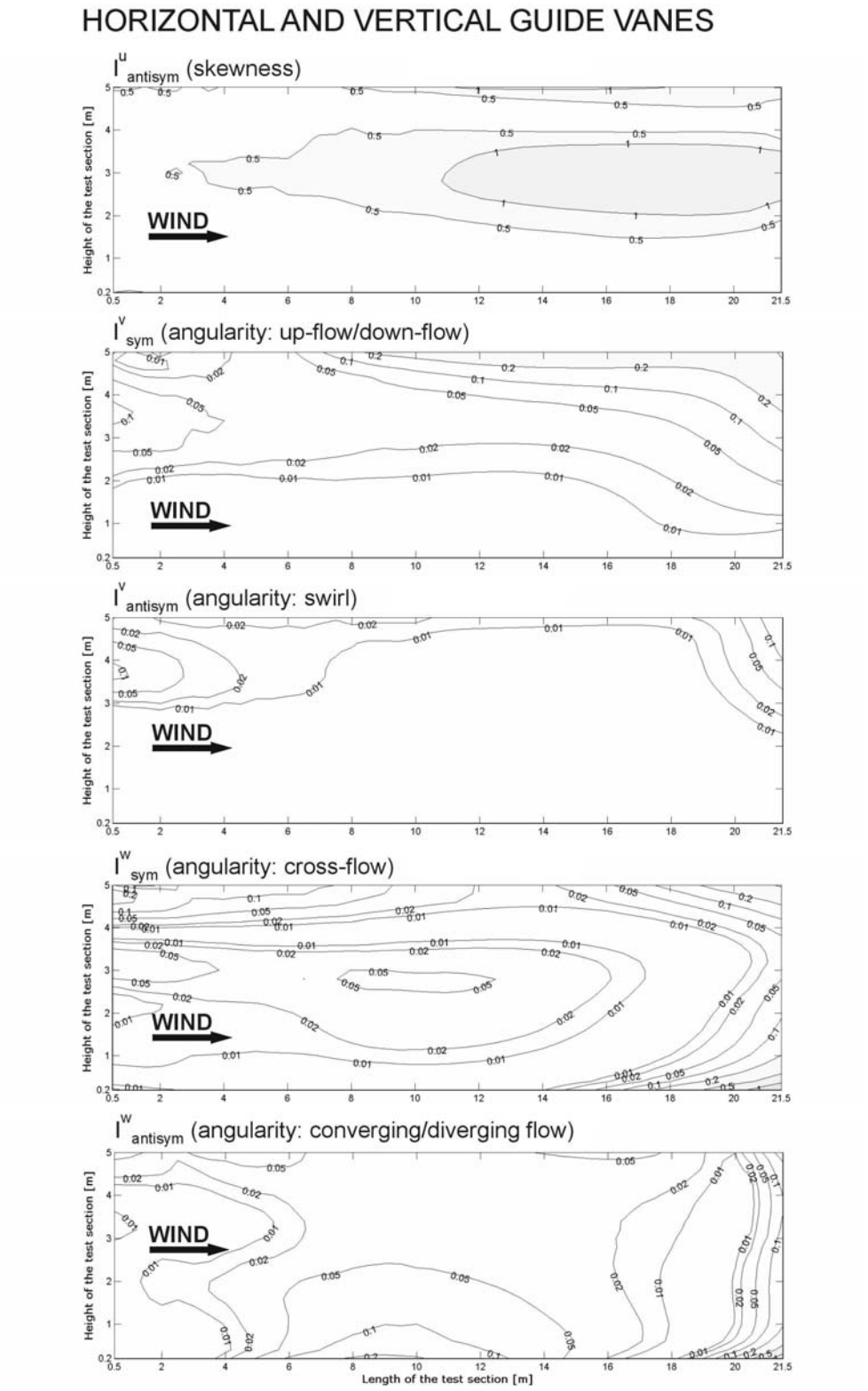
HORIZONTAL AND VERTICAL GUIDE VANES
I u antisym (skewness)
I v sym (angularity: up-flow/down-flow)
I v antisym (angularity: swirl)
I w sym (angularity: cross-flow)
I w antisym (angularity: converging/diverging flow)
WIND
Height of the test section [m]
Length of the test section [m]

Figure 13

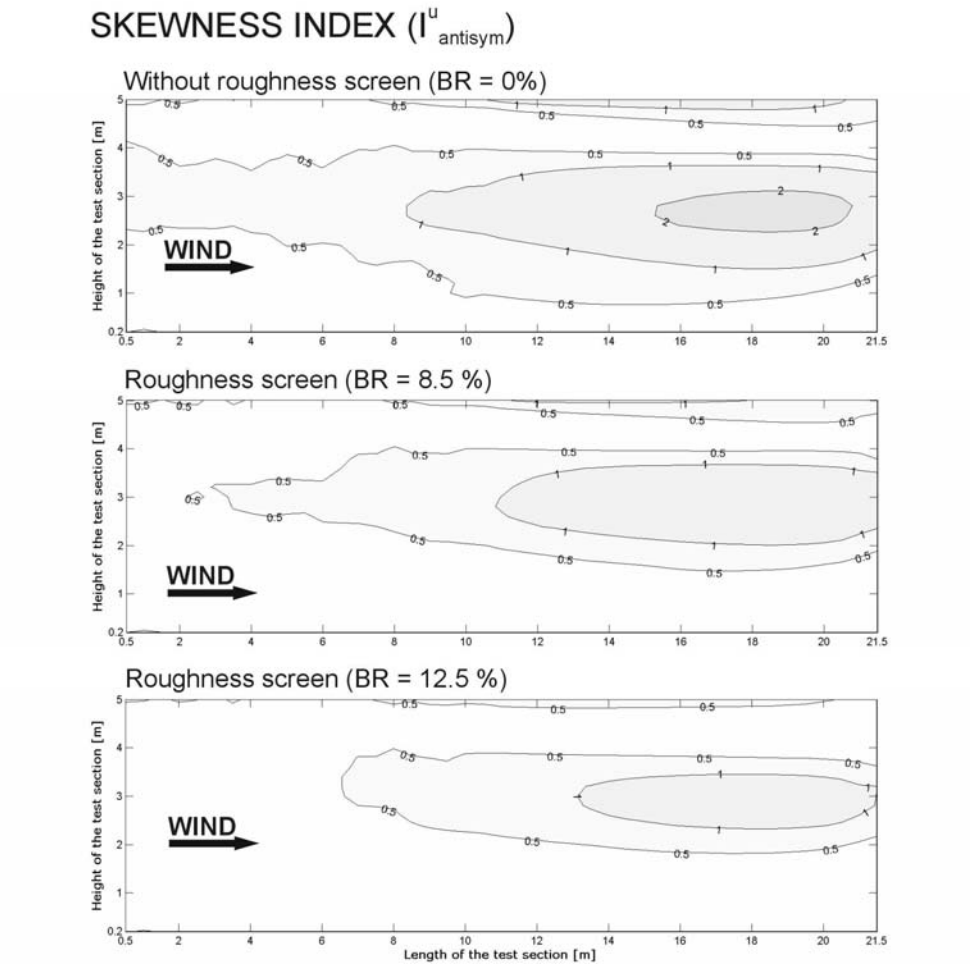
SKEWNESS INDEX ($I^u_{antisym}$)
Without roughness screen (BR = 0%)
Roughness screen (BR = 8.5 %)
Roughness screen (BR = 12.5 %)
WIND
Height of the test section [m]
Length of the test section [m]

Figure 14